Kinetic theory of semiconductor cascade laser based on quantum wells and wires

V. F. Elesin and A. V. Krasheninnikov

Moscow State Institute of Engineering Physics, 115409 Moscow, Russia
(Submitted 4 June 1996)
Zh. Éksp. Teor. Fiz. **111**, 681–695 (February 1997)

The paper presents a numerical solution of a system of nonlinear equations for the electron distribution functions in the upper and lower subbands between which lasing transitions occur and the number of nonequilibrium optical phonons in semiconducting cascade lasers based on quantum wells and wires. For the case of quantum wells, we propose an analytical solution of this system of equations, which is a generalization of the previously found solution [V. F. Elesin and Yu. V. Kopaev, Zh. Éksp. Teor. Fiz. **108**, 2186 (1995) [JETP **81**, 1192 (1995)]; V. F. Elesin and Yu. V. Kopaev, Sol. St. Commun. **96**, 897 (1995)] in a wider range of injection rates. The threshold injection rate can be significantly reduced owing to reabsorption and accumulation of nonequilibrium optical phonons, nonparabolicity of the subbands and different effective masses of electrons in different subbands. In the case of quantum wires, the threshold injection rate is considerably lower, and its decrease is even larger than in quantum wells. It is remarkable that, owing to the lower electron–electron relaxation rate in the one-dimensional case, the decrease in the threshold injection rate may be two or three orders of magnitude. The relation between the density of states and threshold current has also been studied. © *1997 American Institute of Physics.* [S1063-7761(97)02102-1]

1. INTRODUCTION

A new type of semiconductor laser (quantum cascade laser) proposed in the original publications by Kazarinov and Suris[1] has been implemented quite recently.[2,3] The interest in quantum cascade lasers based on electronic transitions between subbands in the conductance band is stimulated by the possibility of tuning them over a wavelength interval extending from the near to far infrared.

Since transitions between subbands due to emission of optical phonons are allowed, quantum cascade lasers are characterized by high threshold currents and highly nonequilibrium states of their electron systems. Specifically, the electron lifetime in the upper subband, equal to the time of optical phonon emission (τ_0), is short ($\tau_0 \approx 10^{-12}$–10^{-13} s) compared to the electron lifetime ($\tau_r \approx 10^{-10}$ s) in conventional semiconductor lasers based on transitions between the conduction and valence bands. As a result, it is difficult to create population inversion in the system and, since the electron system is far from equilibrium, a kinetic approach is indispensable in modeling the electron energy relaxation in such lasers.

In the first experiments with quantum cascade lasers,[2,3] the parameters of a semiconducting heterostructure were selected so that the electron transit time from the lower subband, τ_t, should be shorter than τ_0 in order to create the population inversion. This condition is inevitable if the laser is treated as a two-level system and band nonparabolicity is ignored.[2,4] With due account of the nonparabolicity, however, the situation is radically different.[5,6] In this case, radiative transitions occur in a fairly narrow energy range, so there is no need to satisfy the strict condition $\tau_0 \gg \tau_t$. As a result, full inversion of the subband populations is not necessary. This conclusion was confirmed by experiments shortly afterward.[7]

In addition to the nonparabolicity, another important effect is the considerable drop in the threshold current due to an increase in $\tau_t (\tau_0 \ll \tau_t)$, and accumulation and reabsorption of optical phonons.[5,6] In fact, these effects lead to a longer effective lifetime of electrons in the upper subband, hence a lower injection rate is needed to create conditions for the population inversion.

The calculations[5,6] for the case of quantum wells were based on an exact analytic solution of the system of kinetic equations for the electron distribution functions in the subbands and the number of phonons. The injection rate Q was assumed to be low in this case ($Q\tau_0 \ll 1$, linear approximation).

The aim of the present study was to find a solution of the system of kinetic equations for the electron distribution functions and threshold injection rates (hence the threshold currents) over a wide range of parameters of the kinetic model of the quantum cascade laser. We have studied both the two-dimensional model of a quantum-well laser and the one-dimensional model of a quantum-wire laser. The latter case is especially interesting in that it offers a way to substantially reduce the threshold current (our study has confirmed the feasibility of this effect). This reduction is due to singularities in the electron density of state in a one-dimensional system and a drastically lower electron–electron relaxation rate. Let us recall that, in the one-dimensional configuration of a single-band model, electron–electron scattering does not lead to energy relaxation[8] (this follows from energy and momentum conservation). An important point is that for $\tau_0 \ll \tau_t$ the threshold current is controlled by electron–electron relaxation.[5,6]

The paper is organized as follows. Section 2 describes the model and gives basic solutions. Section 3 presents an exact analytical solution of the system of kinetic equations for electrons and phonons in the quasilinear approximation,

 1063-7761/97/020375-08$10.00

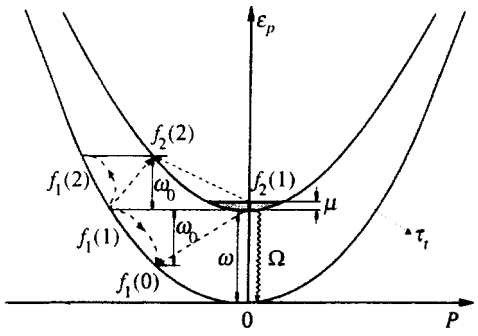

FIG. 1. Energy in the subbands versus quasimomentum. The dashed lines show transitions with emission of an optical phonon, the wavy line shows an optical transition.

which applies to a wide range of Q. Numerical solutions of the initial equation system in the case of quantum wells and their detailed analysis are given in Sec. 4. Section 5 presents a numerical solution of the system of nonlinear kinetic equations for the case of quantum wires.

2. BASIC EQUATIONS AND STATEMENT OF THE PROBLEM

As in the previous studies,[5,6] let us consider the following model (Fig. 1). Let there be two subbands with dispersions $\varepsilon_1(\mathbf{p})$ and $\varepsilon_2(\mathbf{p})$, such that transitions between them are accompanied by emission of phonons with the energy $\hbar\Omega$ (hereafter $\hbar=c=1$, where c is the speed of light in vacuum). Electrons are injected into the subband 2 at a rate Q and drain from the subband 1 with a probability τ_t^{-1}. The optimal conditions for operation of quantum cascade lasers are achieved by selecting the parameters of the quantum wells and barriers of the structure.[2–4]

In the present model, the main scatterers of electrons are optical phonons (the typical energy is $\omega_0\approx 0.034$ eV[7]). At $\mathbf{p}=0$ the difference between the subband energies $\omega=\varepsilon_2(0)-\varepsilon_1(0)$ is approximately several phonon energies ω_0. The parameter μ ($\mu\ll\omega_0$) is the spread of the injected electron energy.

Our main task is to determine the threshold injection rate Q_{th}. It can be derived by equating the gain $\alpha(\Omega)$ and the reciprocal of the photon lifetime τ in the cavity[5,6] controlled by the total losses:

$$\alpha(\Omega_0,J_{\text{th}})=\frac{1}{\tau},\quad \left.\frac{\partial\alpha(\Omega)}{\partial\Omega}\right|_{\Omega=\Omega_0}=0. \tag{1}$$

The latter condition is the equation for the lasing frequency. The expression for $\alpha(\Omega)$ describing electronic transitions between the subbands has the form[5,6]

$$\frac{\alpha(\Omega)}{\alpha_0}=\int_0^\infty \frac{d\varepsilon[f_2(\varepsilon)-f_1(\varepsilon)]\gamma}{(\xi_2(\varepsilon)-\xi_1(\varepsilon))^2+\gamma^2},\quad \alpha_0=\frac{e^2|V_{12}|^2}{\Omega\kappa}, \tag{2}$$

$$\xi_2(\varepsilon)=\varepsilon+\omega-\frac{\Omega}{2},\quad \xi_1(\varepsilon)=\varepsilon+\frac{\Omega}{2}, \tag{3}$$

where $f_2(\varepsilon)$ and $f_1(\varepsilon)$ are distribution functions of electrons in the subbands *2* and *1* (Fig. 1), γ is the damping factor of nondiagonal components of the density matrix (it is assumed to be constant with the energy), Ω is the electromagnetic field frequency, V_{12} is the matrix element of the electronic transition between the subbands, κ is the dielectric constant, and e is the electron charge.

If the band nonparabolicity is ignored, the difference $\xi_2-\xi_1=\omega-\Omega\equiv\delta$ is independent of the energy. In this case, the electronic transitions with emission (or absorption) of photons occur throughout the subband, and the system is equivalent to a conventional two-level system. The lasing condition in this approximation is[2,4]

$$\tau_t<\tau_0, \tag{4}$$

which is necessary to satisfy conditions (1) and (2).

The inclusion of the subbands nonparabolicity changes the situation radically.[5,6] First, the rigorous condition (4) is no longer necessary. Second, it becomes possible to significantly reduce Q_{th} because the subband nonparabolicity limits the lasing spectral range.

If we use the simplest approximation for the GaAs electronic spectrum,[9] the difference $\xi_2-\xi_1$ in the case of a deep quantum well can be expressed as[5,6]

$$\varepsilon_2-\varepsilon_1=\delta-\beta\varepsilon,\quad \beta=2\omega/\varepsilon_g, \tag{5}$$

where ε_g is the band gap width. Later similar results were obtained by Gelmont *et al.*[10] Faist *et al.*[7] studied a more complicated model taking into account features of real structures, and their results are approximately equal to those reported in Refs. 5 and 6 to within 25%.

By taking into account Eq. (5) and assuming that

$$f_2(\varepsilon)-f_1(\varepsilon)=\begin{cases}\Delta f, & 0<\varepsilon<\mu,\\ 0, & \mu<\varepsilon,\end{cases} \tag{6}$$

we derive from Eq. (1) at the resonant frequency

$$\Omega_0=\omega-\frac{\mu\beta}{2},$$

$$\frac{\alpha(\Omega_0)}{\alpha_0}=\frac{2\Delta f}{\beta}\arctan\frac{\mu\beta}{2\gamma}\approx\frac{\Delta f\pi}{\beta}$$

for $\mu\beta\gg 2\gamma$. The threshold population inversion is determined, correspondingly, by the expression

$$\Delta f_{\text{th}}=\frac{\beta}{\pi\tau\alpha_0}. \tag{7}$$

In order to determine Q_{th}, we need the relationship between $f_i(\varepsilon)$ and Q. It can be determined by solving the system of kinetic equations for $f_i(\varepsilon)$ and the number of optical phonons N.

The relevant kinetic equations were derived by Elesin and Kopaev.[5,6] They also reduced the system of equations to a system of coupled equations for the functions $f_1(n)$ and $f_2(n)$, where

$$f_1(n)\equiv f_1(\omega+(n-1)\omega_0)=f_1(\varepsilon),$$

$$f_2(n)\equiv f_2(\omega+n\omega_0)=f_2(\varepsilon),\quad n=0,1,2\ldots$$

The functions $f_1(n)$ and $f_2(n)$ describe the distribution of electrons with energies in a narrow interval $\mu\ll\omega_0$ around

the energies $\varepsilon=\omega\pm n\omega_0$. These equations have the form

$$f_1(0)[\xi+N(1+z)+f_1(1)+zf_2(1)] =(1+N)[f_1(1)+zf_2(1)], \quad (8)$$

$$f_1(0)[\xi+1+N(2+z)-f_1(0)+f_1(2)+zf_2(2)] =Nf_1(0)+(1+N)[f_1(2)+zf_2(2)], \quad (9)$$

$$f_2(1)[Q\tau_0+1+N(2+z)-f_1(0)+f_1(2)+zf_2(2)] =Nf_1(0)+(1+N)[f_1(2)+zf_2(2)]+Q\tau_0, \quad (10)$$

$$f_1(n)[\xi+(1+z)(1+2N)-f_1(n-1)-zf_2(n-1) +f_1(n+1)+zf_2(n+1)] =N[f_1(n-1)+zf_2(n-1)]+(1+N)[f_1(n+1) +zf_2(n+1)], \quad (11)$$

$$f_2(n)[(1+z)(1+2N)-f_1(n-1)-zf_2(n-1)+f_1(n +1)+zf_2(n+1)] =N[f_1(n-1)+zf_2(n-1)]+(1+N)[f_1(n+1) +zf_2(n+1)], \quad (12)$$

where $\xi=\tau_0/\tau_t$, $z=m_2/m_1$ is the ratio between the electron effective masses in the subbands *2* and *1*, respectively. In all our analytical calculations we take $z=1$ (the case $z\neq 1$ is considered in Sec. 4). Equations (11) and (12) are valid for $n\geqslant 2$. The system should be supplemented with an equation for the number N of optical phonons:[5]

$$N\frac{\tau_t}{\tau_{\rm esc}}=f_1(0)-\sum_{n=2}^{\infty}(n-1)f_1(n), \quad (13)$$

where $\tau_{\rm esc}$ is the time in which phonons escape from a region with given dimensions.[5]

Given that the functions $f_2(n)$ are nonzero in a narrow energy interval, the difference $f_2(\varepsilon)-f_1(\varepsilon)$ in Eq. (6) becomes equal to $f_2(1)$ at the generation threshold. Specifically, the electrons emitting optical phonons do not arrive at the bottom of the subband *1*, i.e., $f_1(\varepsilon)=0$ in the region where lasing occurs (Fig. 1), except the case of resonance, when $\omega=k\omega_0$.

3. EXACT ANALYTICAL SOLUTION IN THE QUASILINEAR APPROXIMATION FOR QUANTUM WELLS

An exact analytical solution of the Eqs. (8)–(13) in the approximation linear in f and $Q\tau_0$ was described in Refs. 5 and 6. It was assumed that the linear approximation ($f\ll 1$, $Q\tau_0\ll 1$) applied in a range extending to $Q\sim 1/\tau_0$, since the nonlinear terms in Eqs. (8)–(12), which were omitted in that approximation, were comparable to terms of order $1+3N$, where $N\sim 1$.

Numerical calculations and more accurate analysis, however, have revealed that some terms in the denominators of the expressions for f_i (their formulas are given below) cancel one another, and the linear approximation is valid when $Q\tau_0$ is limited to a quantity of order $\xi\ll 1$, rather than $1+3N\approx 4$.

At the same time, ''dangerous'' denominators that may lead to divergence are caused only by the term proportional to $Q\tau_0 f_2(1)$ on the left-hand side of Eq. (10). If this term is retained (we call this the quasilinear approximation), the linear system of equations derived from Eqs. (8)–(13) has an exact analytical solution in good agreement (see Sec. 4) with the numerical solution to Eqs. (8)–(13).

The solution of the system (8)–(13) in the quasi-linear approximation is as follows:

$$f_1(n)=A_1\,\exp(\alpha n), \quad f_2(n)=A_2\,\exp(\alpha n), \quad n\geqslant 2, \quad (14)$$

$$\widetilde{A}_1=A_1\,\exp(\alpha)=Q\tau_0\,\frac{(\xi+c)b}{(\xi+2b)\widetilde{\Delta}},$$

$$\widetilde{A}_2=A_2\,\exp(\alpha)=Q\tau_0\,\frac{(\xi+b)(\xi+c)}{(\xi+2b)\widetilde{\Delta}}, \quad (15)$$

$$\widetilde{\Delta}=(\xi+c)(c+Q\tau_0)-(1+N)(\xi+2c+Q\tau_0)-(1+N) \times(\xi+2c+Q\tau_0)[\exp(\alpha)+N/(\xi+2N)], \quad (16)$$

$$f_1(0)=Q\tau_0\,\frac{(1+N)(\xi+c)}{(\xi+2N)\widetilde{\Delta}}, \quad (17)$$

$$f_1(1)=Q\tau_0\,\frac{y}{\widetilde{\Delta}}, \quad y=(1+N)\exp(\alpha)+\frac{N(1+N)}{\xi+2N}, \quad (18)$$

$$f_2(1)=Q\tau_0\,\frac{\xi+c-y}{\widetilde{\Delta}}, \quad (19)$$

$$\exp(\alpha)=\frac{b(\xi+b)}{2(1+N)(\xi+2b)} -\sqrt{\left\{\frac{b(\xi+b)}{2(1+N)(\xi+2b)}\right\}^2-\frac{N}{1+N}}, \quad (20)$$

$$b=2(1+2N), \quad c=1+3N.$$

Equations (7) and (14)–(20) yield the threshold injection rate $Q_{\rm th}$ in a general form.

The solution (14)–(20) obtained in the quasilinear approximation differs from the linear solution[5,6] only in the denominator $\widetilde{\Delta}$, which contains $Q\tau_0$. We note that some errors slipped into the equations given in Ref. 5 (for example, Eq. (57) of Ref. 5 should contain $n\geqslant 2$), although these errors did not affect the final results and conclusions. The calculations performed in both linear and quasilinear approximations coincide in the limiting case $\xi\ll 1$, but some differences in numbers emerge for $\xi\gg 1$. Note that the solution (14)–(20) agrees well with numerical calculations (see Sec. 4).

It is interesting to investigate the limiting cases $\xi\ll 1$ and $\xi\gg 1$. In the first case, after expanding in $\xi\ll 1$ ($\xi\ll N$) and performing lengthy calculations, we derive from Eqs. (14)–(20)

$$f_1(0)\approx Q\tau_0\,\frac{1+N}{\xi(1+N)^2+Q\tau_0 N}, \quad (21)$$

$$f_2(1)\approx f_1(1)\approx Q\tau_0\ \frac{1+N}{\xi(1+N)^2+Q\tau_0 N}. \tag{22}$$

We see that $Q\tau_0$ in the denominators of Eqs. (21) and (22) should be compared not with $1+3N$, but with a parameter proportional to ξ. If

$$Q\tau_0<Q_c\tau_0=\xi(1+N)^2/N\sim 4\xi, \tag{23}$$

we obtain Eqs. (72) and (73) from Ref. 5. For $Q>Q_c$ [or $\xi<\xi_c=Q\tau_0 N/(1+N)^2$] the growth in $f_2(1)$ described by Eq. (22) saturates, i.e., $f_2(1)\to 1$.

In the quasilinear approximation, one can easily derive an equation for N:

$$\frac{N}{1+N}=Q\tau_{\rm esc}\ \frac{\xi(1-N^2)}{\xi(1+N)^2+Q\tau_0 N}. \tag{24}$$

For $Q<Q_c$ it transforms to Eq. (74) from Ref. 5. The value of N derived from this cubic equation is substituted into Eq. (22) to obtain $f_2(1)$ as a function of $Q\tau_0$ (see below Fig. 3a). The limit of N at $Q\tau_{\rm esc}\gg 1$ is of order unity (for details see Sec. 4).

Now let us determine the threshold injection rate using Eqs. (7) and (22):

$$Q_{\rm th}(\xi\ll 1)\approx\frac{(1+N)^2}{N\tau_t}\,\frac{q}{1-q}, \tag{25}$$

$q=\beta/\pi\tau\alpha_0$.

We can see that, owing to the effect of optical phonon reabsorption, $Q_{\rm th}$ is determined not by τ_0, but by the effective electron lifetime in the upper subband, $\tau_t N/(1+N)^2$.

Consider the opposite limit $\xi\gg 1$. By expanding in terms of the small parameter $1/\xi$ and assuming $\xi\gg N$, we obtain the following expressions:

$$f_1(0)\approx\frac{Q\tau_0(1+N)}{\xi(a+Q\tau_0)}, \tag{26}$$

$$f_2(1)\approx\frac{Q\tau_0}{a+Q\tau_0}, \tag{27}$$

where $a=N+\sqrt{1+3N+3N^2}$.

The equation for N in this case has the form

$$\frac{N}{Q\tau_{\rm esc}}=\frac{(1+N)(2+N-\sqrt{1+3N+3N^2})}{(\sqrt{1+3N+3N^2}-N)(\sqrt{1+3N+3N^2}+N+Q\tau_0)}. \tag{28}$$

In the case $Q\tau_{\rm esc}\gg 1$, we derive from Eq. (28) the limit of the phonon number N_0:

$N_0=1.5$.

Hence, $a=5$ at $N=N_0$, and the linear approximation is valid for $Q\tau_0\leqslant 5$.

At arbitrary $Q\tau_{\rm esc}$ the number of phonons as a function of $Q\tau_0$ can be determined by solving Eq. (28) numerically. These numerical calculations are shown in Fig. 2. The graph shows that $N_0=1.5$, in agreement with the analytical calculation. The dashed curve in Fig. 2 shows the function $N(Q\tau_0)$ calculated by numerically solving the system of nonlinear equations using the iterative technique (see Sec. 4).

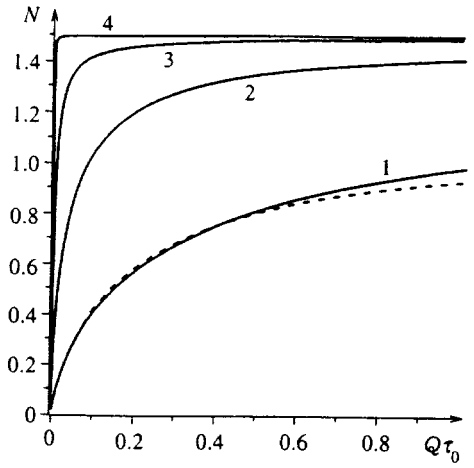

FIG. 2. The number of phonons N versus the injection rate $Q\tau_0$ obtained by solving Eq. (28) numerically. The curves were calculated at (*1*) $\tau_{\rm esc}/\tau_0=10$, (*2*) 10^2, (*3*) 10^3, and (*4*) 10^5. The dashed line corresponds to a numerical solution of nonlinear system of equations (8)–(13) at $\tau_t/\tau_0=0.1$ ($\xi=10$) and $\tau_{\rm esc}/\tau_0=10$.

The solid and dashed curves are very close, which proves that the quasilinear approximation can be used in calculating N.

Let us derive the threshold injection rate in the limit $\xi\gg 1$ from Eqs. (7) and (27):

$$Q_{\rm th}(\xi\gg 1)\approx\frac{5}{\tau_0}\,\frac{q}{1-q}. \tag{29}$$

By comparing Eqs. (25) and (29), we obtain the relation

$$\frac{Q_{\rm th}(\xi\ll 1)}{Q_{\rm th}(\xi\gg 1)}\approx\frac{(1+N)^2}{5N}\,\xi,$$

where $\xi\ll 1$ holds on the right-hand side. Assuming $N\approx 1$, we have an estimate

$$\frac{Q_{\rm th}(\xi\ll 1)}{Q_{\rm th}(\xi\gg 1)}\sim\xi, \tag{30}$$

which is almost identical to Eq. (76) in Ref. 5. It is clear that the threshold injection rate can be reduced proportionally to $\xi=\tau_0/\tau_t$ (for example, by increasing τ_t through the barrier thickness). We should stress that this result is valid for $Q\tau_{\rm esc}\gg 1$, but $Q_{\rm th}$ can be reduced for all $Q\tau_{\rm esc}\geqslant 1$.

4. NUMERICAL SOLUTIONS OF THE SYSTEM OF NONLINEAR KINETIC EQUATIONS FOR THE CASE OF QUANTUM WELLS

We have calculated numerical solutions of the nonlinear equation system (8)–(13) with the parameters $\tau_{\rm esc}$, τ_0, τ_t, and Q varied over wide ranges. This has been done using the iteration technique. On each step of the iteration process, the equation system (8)–(13) was considered as a system of linear algebraic equations, the functions $f_i(n)$ in the brackets on the left-hand side of Eqs. (8)–(13) being constants calculated in the previous iteration. All the times were measured in units of τ_0.

Since $f_2(1)$ determines, in fact, the threshold population inversion, it seems that the shape of this function is more

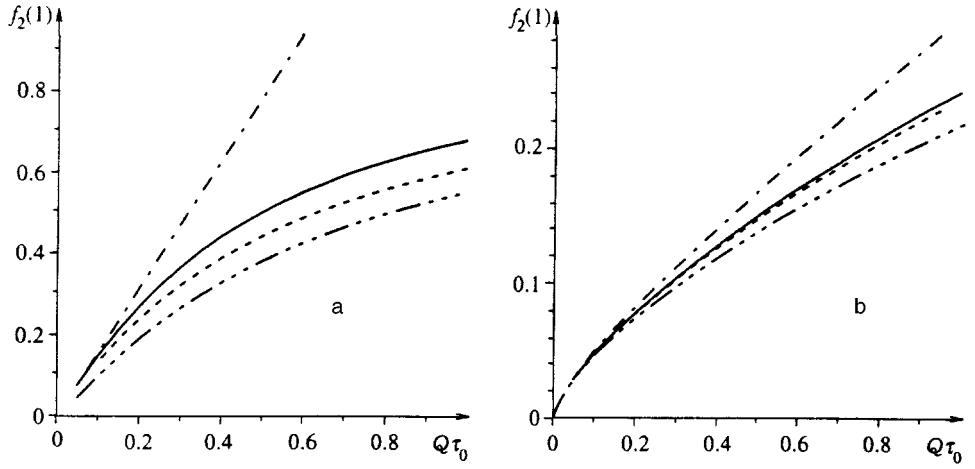

FIG. 3. The function $f_2(1)$ versus the injection rate $Q\tau_0$. The solid curve shows a numerical solution of the nonlinear equation system (8)–(13), the dashed curve a solution of Eqs. (8)–(13) in the quasilinear approximation, and the dash-dotted curve a solution of Eqs. (8)–(13) in the linear approximation. The dash-dotted line with three dots in a row is a calculation from Eq. (22) for the case $\xi=10$ and from Eq. (27) for the case $\xi=0.2$, $\tau_{esc}/\tau_0=10$. (a) $\tau_t/\tau_0=5$ ($\xi=0.2$); (b) $\tau_t/\tau_0=0.1$ ($\xi=10$).

helpful in understanding the system behavior and conveys more information. Figures 3–8 show typical curves of $f_2(1)$ and N as functions of τ_t/τ_0 and $Q\tau_0$.

Figure 3a demonstrates the coincidence among the curves of $f_2(1)$ versus $Q\tau_0$ calculated by Eq. (22) for the limiting case $\xi \ll 1$ (dash-dotted line with three dots in a row), of the numerical solution of Eqs. (8)–(13) in the quasilinear approximation (dashed curve), and of the numerical solution of the equation system (8)–(13) (solid curve). The graph indicates that the solution obtained in the quasilinear approximation is, in fact, identical to the numerical solution in the wide range of $Q\tau_0$, and the solution obtained in the linear approximation has a satisfactory accuracy up to $Q\tau_0 \sim \xi$.

Figure 3b shows similar curves at $\xi=10$. In the limit $\xi \gg 1$ the function $f_2(1)$ versus $Q\tau_0$ was calculated using Eq. (27). It is clear that in the limit $\xi \gg 1$ the analytical solution (27) is in good agreement with the numerical solutions of the nonlinear equation system and with solutions obtained in the linear and quasilinear approximations. Note that in all the limiting cases the quasilinear analytical solution (22), (27) is valid over a wide range of $Q\tau_0$.

Figure 4a shows $f_2(1)$ versus τ_t/τ_0 at $Q\tau_0=0.1$. The curve demonstrates the growth in $f_2(1)$ with τ_t/τ_0, in accordance with the analytical results (22) and (27) (see also Refs. 5 and 6). For example, in the case $Q\tau_0 \ll 1$, $Q\tau_{esc} \gg 1$ (Fig. 3b), we have $f_2(1) \sim 0.027$ at $\tau_t/\tau_0=0.1$ ($\xi=10$) and $f_2(1) \sim 0.25$ at $\tau_t/\tau_0=10$ ($\xi=0.1$). This is in agreement with the main conclusion that the threshold injection rate should decrease with τ_t. Note also that the increase in $f_2(1)$ is not so large at relatively large q/τ_0 [Eqs. (22) and (27)].

Up to this point, we have assumed that the electron masses in the subbands are equal. If we assume that they are different ($m_2 > m_1$), the solid curves with dots in Fig. 4, numerically calculated by solving Eqs. (8)–(13) at $m_2/m_1=1.5$, indicate that $f_2(1)$ becomes larger than for the calculation with equal electron masses (solid curve), all other conditions being equal.

5. NUMERICAL SOLUTIONS OF THE NONLINEAR KINETIC EQUATION SYSTEM FOR THE CASE OF QUANTUM WIRES

As was noted in Introduction, it is interesting to consider a kinetic model of a one-dimensional cascade laser in view of the slower electron–electron relaxation and singularities in the density of states in a one-dimensional system. The system of kinetic equations can be reduced in this case to a system of coupled equations in the form

$$f_1(0)\left[\xi+N\left(\frac{1}{\sqrt{w}}+\frac{x}{\sqrt{2\tilde{\mu}}}\right)+\frac{f_1(1)}{\sqrt{w}}+x\,\frac{f_2(1)}{\sqrt{2\tilde{\mu}}}\right]$$
$$=(1+N)\left[\frac{f_1(1)}{\sqrt{w}}+\frac{f_2(1)}{\sqrt{2\tilde{\mu}}}\right], \tag{31}$$

$$f_1(1)\left[\xi+\frac{1+N}{\sqrt{w-1}}+N\left(x+\frac{1}{\sqrt{w+1}}\right)-\frac{f_1(0)}{\sqrt{w-1}}\right.$$
$$\left.+\frac{f_1(2)}{\sqrt{w+1}}+xf_2(2)\right]$$
$$=f_1(0)\frac{N}{\sqrt{w-1}}+(1+N)\left[\frac{f_1(2)}{\sqrt{w+1}}+xf_2(2)\right], \tag{32}$$

$$f_2(1)\left[Q\tau_0+\frac{1+N}{\sqrt{w-1}}+N\left(x+\frac{1}{\sqrt{w+1}}\right)-\frac{f_1(0)}{\sqrt{w-1}}\right.$$
$$\left.+\frac{f_1(2)}{\sqrt{w+1}}+xf_2(2)\right]$$
$$=f_1(0)\frac{N}{\sqrt{w-1}}+(1+N)\left[\frac{f_1(2)}{\sqrt{w+1}}+xf_2(2)\right]$$
$$+Q\tau_0, \tag{33}$$

$$f_1(2)\left[\xi+\frac{1}{\sqrt{w}}+\frac{x}{\sqrt{2}}+N\left(\frac{1}{\sqrt{w+2}}+\frac{1}{\sqrt{w}}+\frac{x}{\sqrt{2\tilde{\mu}}}+\frac{x}{\sqrt{2}}\right)-\frac{f_1(1)}{\sqrt{w}}-x\,\frac{f_2(1)}{\sqrt{2\tilde{\mu}}}+\frac{f_1(3)}{\sqrt{w+2}}+x\,\frac{f_2(3)}{\sqrt{2}}\right]$$
$$=N\left[\frac{f_1(1)}{\sqrt{w}}+x\,\frac{f_2(1)}{\sqrt{2\tilde{\mu}}}\right]+(1+N)\times\left[\frac{f_1(3)}{\sqrt{w+2}}+x\,\frac{f_2(3)}{\sqrt{2}}\right], \tag{34}$$

$$f_2(2)\left[(1+N)\left(\frac{x}{\sqrt{2\tilde{\mu}}}+\frac{1}{\sqrt{w}}\right)+N\left(\frac{1}{\sqrt{w+2}}+\frac{x}{\sqrt{2}}\right)-\frac{f_1(1)}{\sqrt{w}}-x\,\frac{f_2(1)}{\sqrt{2\tilde{\mu}}}+\frac{f_1(3)}{\sqrt{w+2}}+x\,\frac{f_2(3)}{\sqrt{2}}\right]$$
$$=N\left[\frac{f_1(1)}{\sqrt{w}}+x\,\frac{f_2(1)}{\sqrt{2\tilde{\mu}}}\right]+(1+N)\left[\frac{f_1(3)}{\sqrt{w+2}}+x\,\frac{f_2(3)}{\sqrt{2}}\right], \tag{35}$$

$$f_1(n)\left[\xi+\frac{1}{\sqrt{w+n-2}}+\frac{x}{\sqrt{n}}+N\left(\frac{1}{\sqrt{w+n}}+\frac{1}{\sqrt{w+n-2}}+\frac{x}{\sqrt{n-2}}+\frac{x}{\sqrt{n}}\right)-\frac{f_1(n-1)}{\sqrt{w+n-2}}-x\,\frac{f_2(n-1)}{\sqrt{n-2}}+\frac{f_1(n+1)}{\sqrt{w+n}}+x\,\frac{f_2(n+1)}{\sqrt{n}}\right]$$
$$=N\left[\frac{f_1(n-1)}{\sqrt{w+n-2}}+x\,\frac{f_2(n-1)}{\sqrt{n-2}}\right]+(1+N)\times\left[\frac{f_1(n+1)}{\sqrt{w+n}}+x\,\frac{f_2(n+1)}{\sqrt{n}}\right], \tag{36}$$

$$f_2(n)\left[(1+N)\left(\frac{x}{\sqrt{n-2}}+\frac{1}{\sqrt{w+n-2}}\right)+N\left(\frac{1}{\sqrt{w+n}}+\frac{x}{\sqrt{n}}\right)-\frac{f_1(n-1)}{\sqrt{w+n-2}}-x\,\frac{f_2(n-1)}{\sqrt{n-2}}+\frac{f_1(n+1)}{\sqrt{w+n}}+x\,\frac{f_2(n+1)}{\sqrt{n}}\right]$$
$$=N\left[\frac{f_1(n-1)}{\sqrt{w+n-2}}+x\,\frac{f_2(n-1)}{\sqrt{n-2}}\right]+(1+N)\times\left[\frac{f_1(n+1)}{\sqrt{w+n}}+x\,\frac{f_2(n+1)}{\sqrt{n}}\right], \tag{37}$$

where $\xi=\tau_0/\tau_t$, $x=\sqrt{m_1/m_2}$, $w=\omega/\omega_0$, and $\tilde{\mu}=\mu/\omega_0$. In Eqs. (36) and (37) we have $n\geqslant 3$.

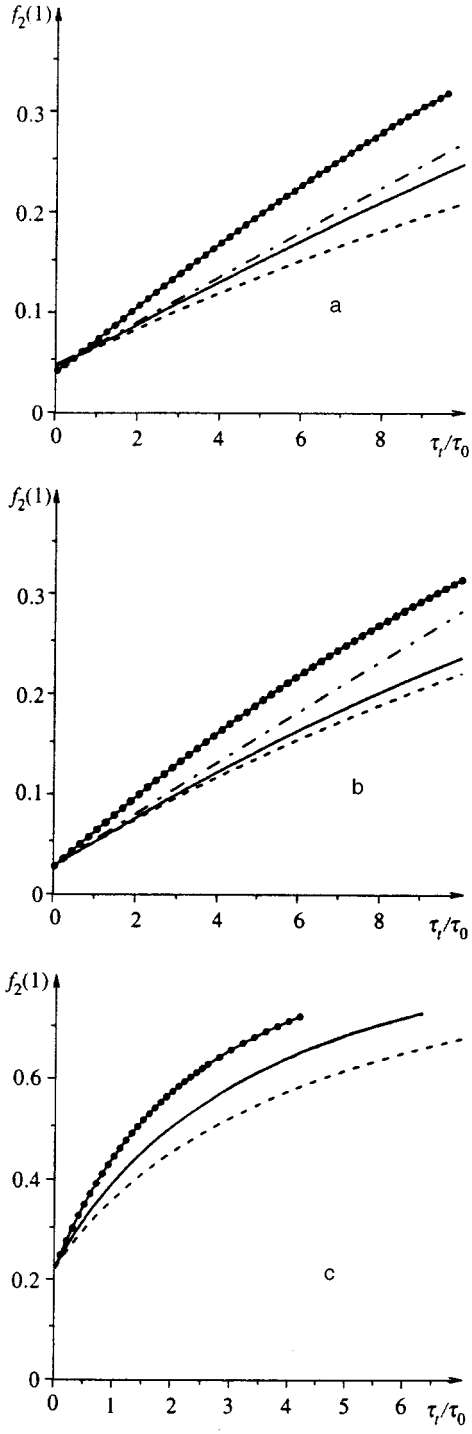

FIG. 4. The function $f_2(1)$ versus τ_t/τ_0. The solid curve shows a numerical solution of the system of nonlinear equations (8)–(13), the dashed line shows a solution in the quasi-linear approximation, the dash-doted line a solution in the linear approximation. The solid line with circles is a numerical solution of Eqs. (8)–(13) for a ratio between the effective masses in the subbands $m_2/m_1=1.5$. (a) $Q\tau_0=0.1$, $\tau_{esc}/\tau_0=10$; (b) $Q\tau_0=0.1$, $\tau_{esc}/\tau_0=100$; (c) $Q\tau_0=1$, $\tau_{esc}/\tau_0=10$.

This equation system should be supplemented with an equation for the phonon number[5] similar to Eq. (13). In the one-dimensional configuration, this equation may differ from the corresponding equations in the two-dimensional [Eq. (13)] and three-dimensional cases. In fact, one can easily

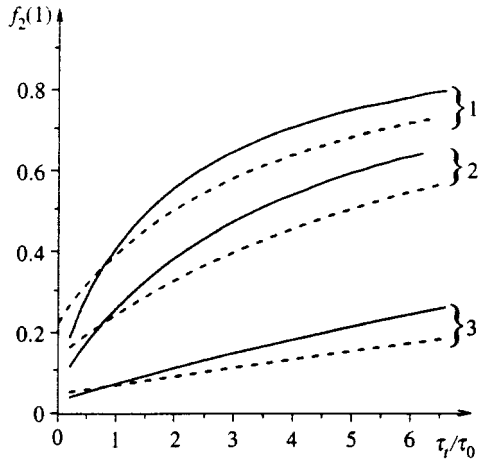

FIG. 5. Curves of $f_2(1)$ versus τ_t/τ_0 for quantum wires (solid lines) and quantum wells (dashed lines). The calculations were performed at (1) $Q\tau_0=1$, (2) 0.5, and (3) 0.1.

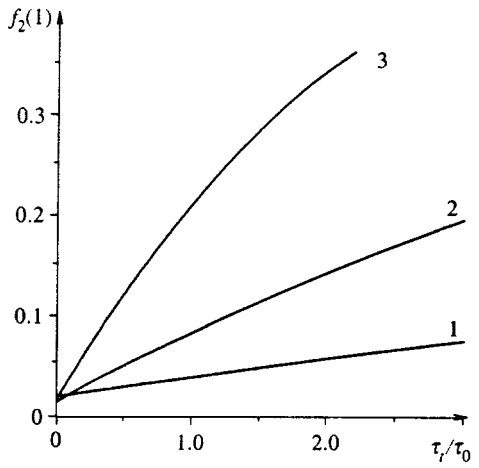

FIG. 7. The function $f_2(1)$ versus τ_t/τ_0 for quantum wires. (*1*) $\mu/\omega_0=0.2$, (*2*) 0.02, and (*3*) 0.002; $Q\tau_0=0.05$.

prove using the energy and momentum conservation that an optical phonon emitted by an electron can impart its energy only to the same electron. Therefore Eq. (13) should be, generally speaking, modified considerably. But in the real situation, when there are several types of optical phonons, these changes may be not so drastic.[11] Taking into account this factor and with a view to simplify the calculation, we use an equation similar to Eq. (13), but with allowance for the electron density of states in the one-dimensional case:

$$N\frac{\tau_t}{\tau_{\rm esc}}\frac{1}{\tilde{\mu}}=\frac{f_1(0)}{\sqrt{w-1}}-\sum_{n=2}^{\infty}\frac{(n-1)f_1(n)}{\sqrt{w+n-1}}. \tag{38}$$

Since the density of state in this case is a function of energy, the system of equations (31)–(38) is more complicated than in the case of quantum wells [Eqs. (8)–(13)], and we could not find an analytical solution. Both systems (31)–(38) and (8)–(13) have been solved by an iteration technique with the parameters $t_{\rm esc}$, τ_0, τ_t, Q, and μ varied over a wide ranges. In all these calculations the electron masses in the subbands were equal.

Figure 5 shows typical curves of $f_2(1)$ versus τ_t/τ_0 at various $Q\tau_0$ (see caption to Fig. 5). For comparison similar curves for the two-dimensional system are also shown. The solid curves show functions calculated numerically for the case of quantum wires, and dashed curves correspond to the case of quantum wells. One can see that in the one-dimensional system, as in the two-dimensional configuration, $f_2(1)$ increases with τ_t/τ_0, and at a higher rate. Thus we conclude that the threshold injection rate in quantum wires decreases with τ_t, and even faster than in quantum wells.

We have also thoroughly investigated $f_2(1)$ as a function of $Q\tau_0$. The curves are shown in Fig. 6. The gain in $f_2(1)$ is higher at small injection rates. It is interesting that for $\tau_t/\tau_0\ll 1$ the gain in $f_2(1)$ for quantum wires is less than for quantum wells.

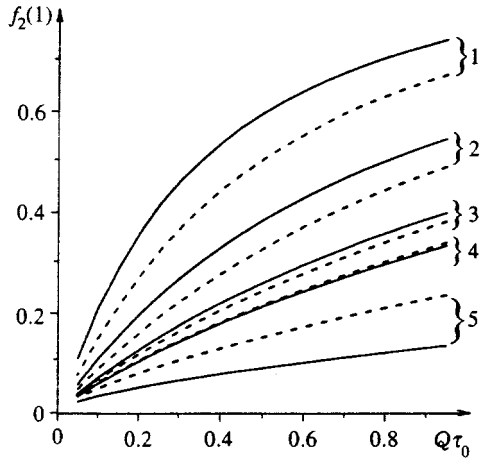

FIG. 6. Curves of $f_2(1)$ versus $Q\tau_0$ for the case of quantum wires (solid lines) and quantum wells (dashed lines). Calculations were preformed at (*1*) $\tau_t/\tau_0=5$, (*2*) 2, (*3*) 1, (*4*) 0.7, and (*5*) 0.1.

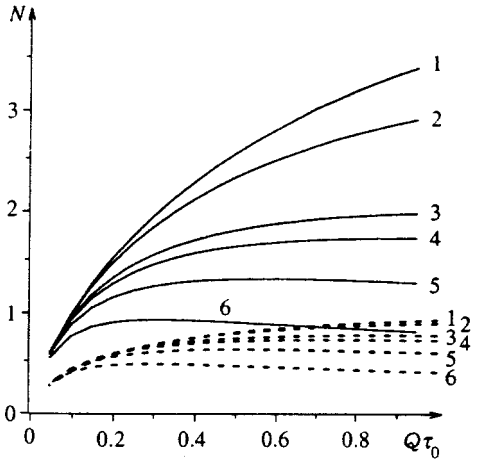

FIG. 8. The number of phonons N versus $Q\tau_0$ for the case of quantum wires (solid lines) and quantum wells (dashed lines). The curves were calculated at (*1*) $\tau_t/\tau_0=0.1$, (*2*) 0.2, (*3*) 0.7, (*4*) 1, (*5*) 2, and (*6*) 5.

The effect of the density of states is illustrated by Fig. 7, which shows $f_2(1)$ versus τ_t/τ_0 for various energy spreads μ of the injected electrons. If the electron energy distribution is narrower, the parameter $f_2(1)$ grows faster with τ_t/τ_0 owing to the singularity in the density of states described in Eqs. (31)–(35) by the terms proportional to $1/\sqrt{\tilde{\mu}}$.

The difference in $f_2(1)$ between two- and one dimensional systems is probably caused by the difference in the numbers of phonons in wires and wells for equal model parameters. This is illustrated by Fig. 8, which shows N as a function of $Q\tau_0$ at different τ_t (see caption to Fig. 8). Figure 8 demonstrates that in both quantum wells and quantum wires N rapidly saturates with the growth of the injection rate at $\tau_t<1$ ($N\sim 1$ even though $Q\tau_0 \ll 1$) because at large τ_t energy is accumulated not only by phonons, but also by the electrons of the lower subband.

6. CONCLUSION

Thus, numerical solutions of the system of nonlinear equations for the electron distribution functions $f_1(n)$ and $f_2(n)$ and the number of phonons N have confirmed the main conclusions of Refs. 5 and 6 about the possibility of reducing the threshold injection rate (threshold current) and about the kinetics of a quantum cascade quantum-well laser. We have determined $f_1(n)$, $f_2(n)$, and N with the model parameters and injection rate Q varied over wide intervals, and limits within which the linear approximation[5,6] applies. We have proved that the linear approximation is valid for $Q<Q_c$ [see Eq. (23)], where $Q\sim\xi$, i.e., in a relatively narrow range for $\xi\ll 1$ and over a wider range for $\xi\gg 1$.

On the other hand, the analytical solution in the quasilinear approximation described in the paper can be used over a wide interval of Q with good accuracy. Using this solution, one can obtain the threshold injection rate Q_{th} both in the general case and in specific limiting cases, and prove that, if phonons are accumulated ($Q\tau_{\text{esc}}\gg 1$), the threshold injection rate Q_{th} can be reduced notably and is controlled only by electron–electron and electron–phonon scattering. Note that estimates of τ_{esc} present some problems. The phonon decay rate $1/\tau_{\text{esc}}$ is determined by its departure from the active region (this time is evidently long, 10^{-8}–10^{-9} s[5,6]) and its decay into acoustic phonons. The latter process is faster. Its time is difficult to estimate, but it is probably considerably longer than τ_0.

The features of the electron kinetics in two-dimensional quantum cascade lasers are also typical of quantum-wire lasers. The exact numerical solutions of the respective kinetic equation system demonstrate that by increasing τ_t it is possible to reduce the threshold current even more than in a quantum-well laser.

Furthermore, τ_t in a quantum-wire laser can be increased to a higher value (10^{-10} s) owing to the lower intrasubband electron–electron relaxation rate,[8] so the threshold current may be two or three orders of magnitude lower.

The threshold current can be additionally reduced owing to singularities in the electron density of states and different effective masses in the subbands. To sum up, it is possible that quantum-wire lasers using transitions between subbands in the conductance band will have threshold currents comparable to those of conventional quantum-well lasers based on the transitions between the conductance and valence bands.

We are indebted to Yu. V. Kopaev for helpful discussions. The work was a part of the Physics of Solid-State Nanostructures Program sponsored by the Ministry of Science and Technology of Russia (grant No. 1-092/4), and was partially supported by the Russian Fund for Fundamental Research (Grant No. 96-02-17363a) and INTAS (Grant No. 93-1704-ext).

[1] A. F. Kazarinov, and R. A. Suris, Fiz. Tekh. Poluprovod. **5**, 797 (1971) [Sov. Phys. Semicond. **5**, 707 (1971)]; Fiz. Tekh. Poluprovod. **6**, 148 (1972) [Sov. Phys. Semicond. **6**, 120 (1972)]; Fiz. Tekh. Poluprovod. **7**, 488 (1973) [Sov. Phys. Semicond. **7**, 347 (1973)].
[2] J. Faist, F. Capasso, D. Sivco *et al.*, Science **264**, 553 (1994); Appl. Phys. Lett. **65**, 2901 (1994).
[3] J. Faist, F. Capasso, C. Sirtori *et al.*, Appl. Phys. Lett. **66**, 538 (1995); J. Faist, F. Capasso, C. Sirtori *et al.*, Appl. Phys. Lett. **67**, 3057 (1995).
[4] C. Sirtori, J. Faist, F. Capasso *et al.*, Appl. Phys. Lett. **68**, 1745 (1996).
[5] J. Faist, F. Capasso, C. Sirtori *et al.*, Phys. Rev. Lett. **76**, 411, (1996).
[6] A. S. Aleksandrov and V. F. Elesin, Zh. Éksp. Teor. Fiz. **58**, 1062 (1970) [Sov. Phys. JETP **31**, 571 (1970)].
[7] E. O. Kane, J. Phys. Chem. Sol. **1**, 249 (1957).
[8] B. Gelmont, V. Gorfinkel, and S. Luryi, Appl. Phys. Lett. **68**, 2171 (1996).
[9] R. Mickevicius, R. Gaska, V. Mitin *et al.*, Semicond. Sci. Technol. **9**, 886 (1994).

Translation was provided by the Russian Editorial office.